JOURNAL OF AIRCRAFT
Vol. 53, No. 4, July-August 2016

F/A-18 Twin-Tail Buffet Modeling Using Nonlinear Eddy Viscosity Models

Ahmed Elmekawy,* Osama A. Kandil,† and Oktay Baysal‡
Old Dominion University, Norfolk, Virginia 23529

DOI: 10.2514/1.C033482

Several fighters suffer from tail buffet problems. The buffet phenomenon is the oscillation of aircraft surface components excited as a result of the interaction between the differential pressures associated with turbulent airflow, aircraft structures, and control surfaces. This paper presents the modeling and simulation of a steady-state one-way and two-way fluid–structure interaction for the tail buffet problem of an F/A−18 fighter. The commercial software ANSYS is used to conduct the simulations. The unsteady Reynolds-averaged Navier–Stokes equations with four turbulent models are used to model the fluid domain. Simulation results of two nonlinear eddy viscosity turbulence models were compared with those of two linear viscosity turbulence models and the experimental data. The two linear turbulence models are standard linear Wilcox k-ω and Spalart–Allmaras. The two nonlinear eddy viscosity models are nonlinear eddy viscosity model and Spalart–Allmaras model with rotation and rotation/curvature corrections. The nonlinear eddy viscosity model is based on the standard linear Wilcox k-ω model and uses the formulation of an explicit algebraic Reynolds stress model. The Spalart–Allmaras model with rotation and rotation/curvature corrections turbulence model is the modified Spalart–Allmaras model with a strain-vorticity-based production and curvature treatment. The finite element analysis to model the structural components was conducted by using shell elements. Based on the simulation results, it is concluded that the buffet problem could be simulated as a two-way fluid–structure interaction and by using the nonlinear eddy viscosity model turbulence model as those give better results than the other considered models.

Nomenclature

a_{ij}	=	anisotropic component of Reynolds stress tensor
$a_{ij}^{(\mathrm{ex})}$	=	extra anisotropic component of Reynolds stress tensor for NLEVM model
C_{b1}	=	model constant for Spalart–Allmaras turbulence model
C_{prod}	=	model constant for SAR turbulence model
C_{μ}^{eff}	=	effective eddy viscosity coefficient for NLEVM model
C_{τ}	=	model constant for NLEVM model
c_{r1}, c_{r2}, c_{r3}	=	model constants for SARC turbulence model
c_{w1}	=	model constant for Spalart–Allmaras turbulence model
D, $\tilde{D}$	=	model constants for SARC turbulence model
f_{r1}	=	rotation function for SARC turbulence model
I	=	identity matrix
k	=	anisotropic component of Reynolds stress tensor
M	=	Mach number
P	=	pressure
P_k	=	production term in k equation
Re	=	Reynolds number
S	=	magnitude of vorticity; magnitude of strain-rate tensor
S_{ij}	=	strain-rate tensor
$\bar{S}_{ij}$	=	mean strain-rate tensor
$\tilde{S}$	=	local deformation rate
$\boldsymbol{U}_i$	=	mean flow velocity vector
$\boldsymbol{u}_i$	=	instantaneous velocity vector
$\bar{\boldsymbol{u}}_i$	=	time-averaged velocity vector
u_i'	=	turbulent fluctuating velocity
x, y, z	=	Cartesian coordinates
II_{Ω}, IV	=	invariants of strain-rate and rotation tensors
α	=	angle of incidence (attack), model constant for k-ω model
β_n	=	model coefficient for NLEVM model
β^*	=	closure coefficient for k-ω model
δ_{ij}	=	Kronecker delta, δ_{ij} is equal to 1 if i is equal to j, and δ_{ij} is equal to 0 if i is not equal to j
$\epsilon_{i,j,k}$	=	alternating symbol
μ	=	molecular viscosity
μ_T	=	turbulent eddy viscosity
υ	=	kinematic viscosity, ν is equal to μ/ρ
$\tilde{\upsilon}$	=	Spalart–Allmaras equation working variable
ρ	=	density
τ	=	turbulent time scale
τ_{ij}	=	viscous stress tensor
ω	=	dissipation per unit turbulence kinetic energy
Ω	=	magnitude of rotation sensor
Ω_{ij}	=	rotation tensor
$\bar{\Omega}_{ij}$	=	mean rotation tensor
Ω_m^{Rot}	=	rotation tensor with respect to the reference frame

Presented as Paper 2014-2447 at the 44th AIAA Fluid Dynamics Conference, Atlanta, GA, 16–20 June 2014; received 2 April 2015; revision received 1 October 2015; accepted for publication 1 October 2015; published online 23 December 2015.

*Graduate Student, Department of Mechanical and Aerospace Engineering. Student Member AIAA.
†Professor and Eminent Scholar, Department of Mechanical and Aerospace Engineering. Associate Fellow AIAA.
‡Dean, Professor, and Eminent Scholar, Batten College of Engineering and Technology. Associate Fellow AIAA.

I. Introduction

STRUCTURAL vibration modes of aircraft surfaces are excited as a result of the interaction between the differential pressures associated with turbulent airflow and aircraft structures and control surfaces. This aeroelastic phenomenon is commonly referred to as buffet. Buffet-induced vibrations have been problematic for aircraft for many years [1] and, if not addressed, can lead to the failure of structural components. Buffet has been a costly problem, not solely in terms of the expense of repairing and replacing aircraft components [2], but also in terms of the impact it has had on mission availability and performance because it forces a restriction on the angle of attack and speed at which certain maneuvers could be flown [3]. Buffet affects a wide range of aircraft and aircraft structures, but its impact has proven to be particularly troublesome for twin-tail fighter aircraft.

Because twin-tail configuration is selected for most of the fifth-generation fighters, more research should be conducted for a better understanding of the physics of the vortical flow over delta wing and the corresponding tail buffet.

For F/A-18 aircraft, early in the service deployment, cracks were discovered on the root stub structure due to buffeting, which led to fatigue damage of the vertical fin, and a special inspection was recommended every 200 flight hours to monitor structural damage due to buffet loads, contributing to high maintenance costs and safety problems [4].

II. Method

The choice of the turbulence model to use for the CFD rendering of the vortex flow is critical to the success of understanding and controlling the buffet [5]. The current approaches, in increasing complexity, range from inviscid, laminar, unsteady Reynolds-averaged Navier–Stokes (URANS), detached eddy simulation (DES), and large eddy simulation to the direct numerical simulation method. The trade-off between computational resources and the solution fidelity, when compared with experimental data, affects the choice of the turbulence model. URANS is used in the present simulations. URANS can predict the secondary separation successfully. However, it predicts a higher level of the turbulence in the vortex core, which leads to a failure in predicting the vortex breakdown. Some treatments to the turbulence models [6] can limit the production term in the strain tensor in vortex core. Gordnier [7] concluded that the linear k-ω turbulence model predicted an excessive amount of eddy viscosity in the vortex core that led to weaker vortices, and it was recommended not to use the linear turbulence model for this type of flow.

Wallin and Johansson [8] and Hellsten [9] proposed a modification to the standard linear k-ω turbulence model for vortical flows by using a nonlinear eddy viscosity model (NLEVM). This NLEVM is based on an explicit algebraic Reynolds stress model by adding an extra anisotropic Reynolds stress term to Boussinesq's assumption. An increase of the dependence of the NLEVM model behavior on the mean rotation tensor has been achieved. Dol et al. [10] concluded that the NLEVM is recommended for capturing the vortical flow over delta wings. Schiavetta and Badcock [11] concluded that the NLEVM turbulence model could capture the flow characteristics with acceptable accuracy when compared with DES results for the same grid and predict buffet response because it captures the main frequencies of the flow.

To solve the problem of the higher eddy viscosity around the primary vortex core, some modifications to the Spalart–Allmaras turbulence model were proposed by Dacles-Mariani et al. [12,13], Spalart and Shur [14], and Shur et al. [15]. These modifications are based on reducing the turbulent eddy viscosity in high rotational flows. Morton et al. [16] indicated that Spalart–Allmaras (SA) turbulence model is unable to resolve the majority of the frequency content of the steady-state results. Morton showed that the Spalart–Allmaras model with a rotation correction (SARC) turbulence model showed an improved spectrum before breakdown, but it did not capture the mid to high frequencies after the breakdown.

A. Nonlinear Eddy Viscosity Model

Wallin and Johansson [8] and Hellsten [9] proposed a modification to the standard linear Wilcox k-ω turbulence model by using an NLEVM. This NLEVM is based on an explicit algebraic Reynolds stress model by adding extra anisotropic Reynolds stress term to the Boussinesq approximation. An increase of the dependence of the NLEVM model behavior on the mean rotation tensor has been achieved. More details can be found in [10,17–19].

An extra term is introduced to the calculation of the anisotropic Reynolds stresses as defined by the Boussinesq approximation:

$$a_{ij} = 2\mu_T \bar{S}_{ij} + a_{ij}^{(\mathrm{ex})} \tag{1}$$

where the viscous strain-rate tensor S_{ij} is given by

$$S_{ij} = \frac{1}{2}\left(\frac{\partial u_i}{\partial x_j} + \frac{\partial u_j}{\partial x_i}\right) \tag{2}$$

and the rotation tensor is given by

$$\Omega_{ij} = \frac{1}{2}\left(\frac{\partial u_i}{\partial x_j} - \frac{\partial u_j}{\partial x_i}\right) \tag{3}$$

The extra term $a_{ij}^{(\mathrm{ex})}$ creates a nonlinear relationship for the Reynolds stresses due to its dependence on both the mean strain-rate and rotational tensors. The equation for the Reynolds stresses then is as follows:

$$\overline{u_i' u_j'} = k\left(\frac{2}{3}\delta_{ij} - 2\mu_T \bar{S}_{ij} + a_{ij}^{(\mathrm{ex})}\right) \tag{4}$$

In this model, the mean strain-rate and rotation tensors are normalized by the turbulent time scale τ; that is, $S = \tau\bar{S}_{ij}$ and $\Omega = \tau\bar{\Omega}_{ij}$, where

$$\tau = \max\left\{\frac{1}{\beta^*\omega}, C_\tau\sqrt{\frac{\mu}{\beta^* k\omega}}\right\} \tag{5}$$

The extra anisotropy term is a reduction of the general form of a_{ij} used in explicit Reynolds stress models, which contains 10 tensorally independent terms. The reduced form, with tensor subscripts omitted, is

$$a^{(\mathrm{ex})} = \beta_3\left(\Omega^2 - \frac{1}{3}II_\Omega I\right) + \beta_6\left(S\Omega^2 + \Omega^2 S - II_\Omega S - \frac{2}{3}IVI\right) + \beta_9(\Omega S\Omega^2 - \Omega^2 S\Omega) \tag{6}$$

where I is the identity matrix, equivalent to δ_{ij}. II_Ω, and IV are two of the independent invariants of S and Ω. The model constants are detailed in [9].

In addition to introducing this new anisotropic term, the calculation of the turbulent eddy viscosity is also modified from the k-ω model and takes the following form:

$$\mu_T = C_\mu^{\mathrm{eff}} \rho k\tau \tag{7}$$

where

$$C_\mu^{\mathrm{eff}} = -\frac{1}{2}(\beta_1 + II_\Omega\beta_6) \tag{8}$$

From this definition of the turbulent eddy viscosity, it is clear that the behavior of the rotation tensor is also taken into account.

To consider the behavior of this model in the prediction of vortical flows, the production of turbulence should again be considered. This also now has an additional term and takes the following form:

$$P_k = (2\mu_T \bar{S}_{ij} - a_{ij}^{(\mathrm{ex})})\bar{S}_{ij} \tag{9}$$

From this relationship, the extra term clearly acts to reduce the turbulent production from the original model. The value of the extra anisotropy will increase and, therefore, reduce the turbulence within the vortex core. The levels of turbulent eddy viscosity also decrease in this region, further reducing the levels of turbulence in the flow.

To select this correction in the codes used herein, Fluent, we choose WJ-BSL-EARSM option under the k-omega model in the k-omega dialog box [20].

B. Spalart–Allmaras Model with Rotation and Rotation/Curvature Corrections

Morton et al. [16,21] studied the vortical flow over a 70 deg semispan delta wing and compared SA, SARC, Menter's shear stress transport model (SST), and DES computations with the experimental

data. Morton indicated that SA and SST turbulence models are unable to resolve the majority of the frequency content of the steady-state results. Although SARC showed an improved spectrum before breakdown, it did not capture the mid to high frequencies after the breakdown. Moreover, DES showed more accurate results of the vortex breakdown behavior.

Corrections proposed to enable SA model to predict the vortical flow behavior were for the rotation and rotation/strain. Both of these two corrections are used in the present simulations.

1. Spalart–Allmaras Model with Rotation Corrections

Dacles-Mariani et al. [12,13] proposed a correction for the SA model to reduce the turbulent eddy viscosity in high rotational flows such as a vortical flow. The reduction in the eddy viscosity production was done by reducing the production of eddy viscosity in which the measure of vorticity was greater than that of strain rate. In this modification

$$S = |\Omega_{ij}| + C_{\text{prod}} \min(0, |S_{ij}| - |\Omega_{ij}|) \tag{10}$$

where

$$C_{\text{prod}} = 2.0, \qquad |\Omega_{ij}| = \sqrt{2\Omega_{ij}\Omega_{ij}}, \qquad |S_{ij}| = \sqrt{2S_{ij}S_{ij}} \tag{11}$$

where S_{ij} is given by Eq. (2).

To select this correction in the codes used herein, Fluent, we choose strain/vorticity production option under SA production in the SA dialog box [20].

2. Spalart–Allmaras Model with Rotation/Curvature Correction

A modification of the production term $C_{b1}\tilde{v}\tilde{S}$ for the SA model was proposed by Spalart and Shur [14] and Shur et al. [15], to account for the rotation and curvature, by reducing the turbulent eddy viscosity in regions with high vorticity. The modification includes multiplying the production term $C_{b1}\tilde{v}\tilde{S}$ of the SA model by the rotation function f_{r1}:

$$f_{r1} = (1 + c_{r1})\frac{2r^*}{1 + r^*}(1 - c_{r3}\tan^{-1}(c_{r2}\tilde{r})) - c_{r1} \tag{12}$$

where

$$r^* = \frac{S}{\Omega} = \frac{\sqrt{2S_{ij}S_{ij}}}{\sqrt{2\Omega_{ij}\Omega_{ij}}} = \sqrt{\frac{S_{ij}S_{ij}}{\Omega_{ij}\Omega_{ij}}} \tag{13}$$

$$\tilde{r} = \frac{2\Omega_{ik}S_{jk}}{\tilde{D}}\left[\frac{DS_{ij}}{Dt} + (\varepsilon_{imn}S_{jn} + \varepsilon_{jmn}S_{in})\Omega_m^{\text{Rot}}\right] \tag{14}$$

$$\tilde{D} = D^4 = [(S_{ij}S_{ij} - \Omega_{ij}\Omega_{ij})]^2 \tag{15}$$

and S_{ij} is given by Eq. (2), and Ω_{ij} in Eq. (3) is modified as follows:

$$\Omega_{ij} = \frac{1}{2}\left(\frac{\partial u_i}{\partial x_j} - \frac{\partial u_j}{\partial x_i}\right) + 2\varepsilon_{mji}\Omega_m^{\text{Rot}} \tag{16}$$

DS_{ij}/Dt is the components of the Lagrangian derivative of the strain rate tensor and all the derivatives should be defined with respect to the reference frame Ω^{Rot}. The reference frame Ω^{Rot} should be used only if the reference frame itself is rotating.

To select this correction in the code, Fluent, we choose curvature correction under options in the SA dialog box [20].

III. Numerical Solution Details

The structural and CFD modeling are performed using ANSYS, ver. 14. The structural modeling is performed by using ANSYS mechanical and finite element technique. The Newmark time integration implicit method is used. Shell elements have been used to model the tails. The consistent mass matrix and no structural damping were used. For CFD modeling of the present cases, the commercial CFD code FLUENT was used to simulate the fluid domain. The URANS equations with four turbulence models have been considered. The turbulence models are standard linear Wilcox k-ω, NLEVM, SA, and Spalart–Allmaras model with rotation and rotation/curvature corrections (SARRC). The temporally first-order implicit, spatially second-order upwind, unsteady solver was used with the incompressible pressure-based segregated solver, using the pressure-coupled algorithm for pressure–velocity coupling. For the fluid–structure interaction interface, each data transfer between the fluid and structure interface incorporates two algorithmic components: mapping and interpolation [22]. The normal and tangential force was transmitted by the conservative and consistent fluid–structure interface algorithm to the tails and the deflections of the tail were transmitted back to the fluid. The interfaces transmit the normal and tangential forces from the fluid grid to the structure grid in a conservative manner.

A mesh dependency study was performed for the structural dynamics mesh of the two tails using three different meshes. Table 1 shows the maximum deflection and Von-Mises stress for three different grids. The second mesh, 200,411 elements, was selected for the present simulations due to its convergence with the third mesh.

A mesh dependency study was conducted for the fluid dynamics mesh using two meshes of varying cell number. Each mesh was processed using the NLEVM turbulence model and steady-state case for 300 iterations. The first mesh consists of 3,807,924 elements. The refined mesh consists of 4,297,360 elements. A comparison of the pressure on the wing upper surface at a distance of 0.13 m from the tip for both meshes is shown in Fig. 1. From Fig. 1, no further refinement was required. The mesh of 3,807,924 elements will be used in the present simulation.

The experimental data used for comparisons are from Washburn et al. [23,24]. Washburn et al. used a simplified geometry of subsonic flow at Mach 0.3 over a 76 deg delta wing at 30 deg angle of attack. Two vertical tails were placed downstream of the delta wing. Washburn et al. showed similarities between the buffet flow characteristics of the simplified geometry and the F/A-18 flight test data. Meyn et al. [25] showed that the subscale tests are adequate for estimating the characteristics of the differential pressure on the tail. Moses and Pendleton [26] showed the largest tail buffet response of F/A-18 simplified model happened at a Mach number 0.3 and at an angle of attack of 30 deg.

IV. Fluid–Structure Interaction Simulation Results

A. Results for Steady RANS, One-Way Fluid–Structure Interaction Case

The results of the present modeling and simulation are for the time-averaged, one-way fluid–structure interaction and two-way fluid–structure interaction for the tail buffet of F/A-18. They are compared with experimental data for steady state.

Presented in Fig. 2 are comparisons of the SARRC- and NLEVM-generated vortex core trajectories with experimental data. The vortex core was computed by locating the center of the vortex in total pressure contours of the flow at different cross flow planes. The

Table 1 Structural mesh dependency study results

	Mesh 1	Mesh 2	Mesh 3
Number of elements	8,233	200,411	537,339
Number of nodes	15,785	341,394	834,694
Max total deformation, mm	1.643	1.658	1.66
Max Von-Mises stress, MPa	6.3836	6.3053	6.3234

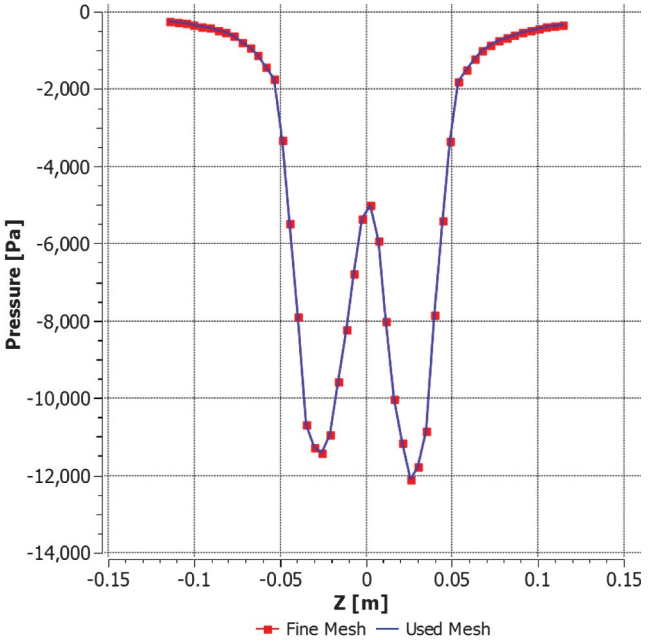

Fig. 1 Fluid mesh comparison of the pressure distribution on the upper surface of the wing at a distance of 0.13716 m from the wing tip. One-way fluid–structure interaction case.

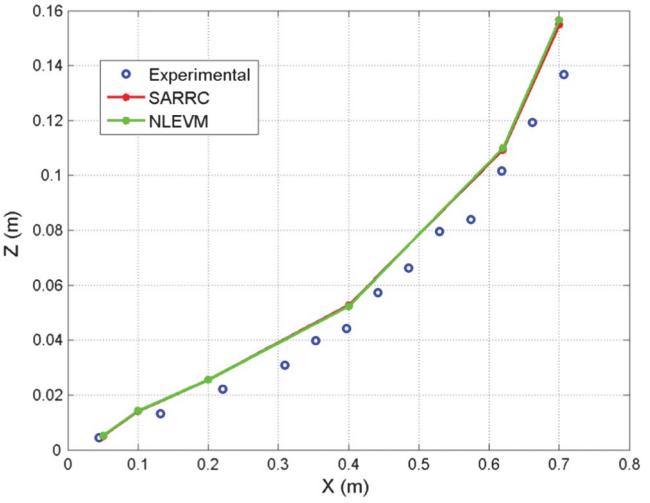

Fig. 2 Vortex core trajectories.

agreement between the experimental and numerical data for the trajectories of the vortex core is very good.

Figure 3 shows the total pressure contours for the upper surface of the wing using SARRC and NLEVM turbulence models. Again, the agreement is very good. The increase of the total pressure indicates the vortex breakdown. The breakdown of the two vortices is symmetric. The vortex breakdown locations are almost the same for both turbulence models.

Figures 4–7 show the snapshots of total pressure contours at four different cross flow planes using SARRC and NLEVM turbulence models. The flow structure can be viewed rather clearly. As flow moves downstream, the enlargement and weakening of the vortices can be observed. The two wing vortices impinge on the two tails. Good agreement between the two turbulence models is clear.

The unsteady nature of the physical flow and the effect of tails movements on the flow are not considered in these one-way fluid–structure interaction and steady computations.

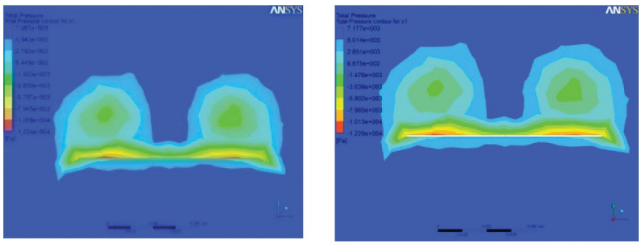

SARRC NLEVM

Fig. 4 Total pressure contours at $x = 0.2$ m.

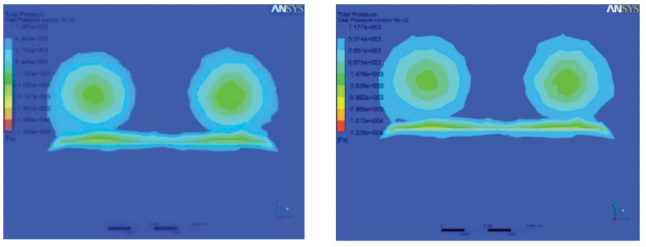

SARRC NLEVM

Fig. 5 Total pressure contours at $x = 0.4$ m.

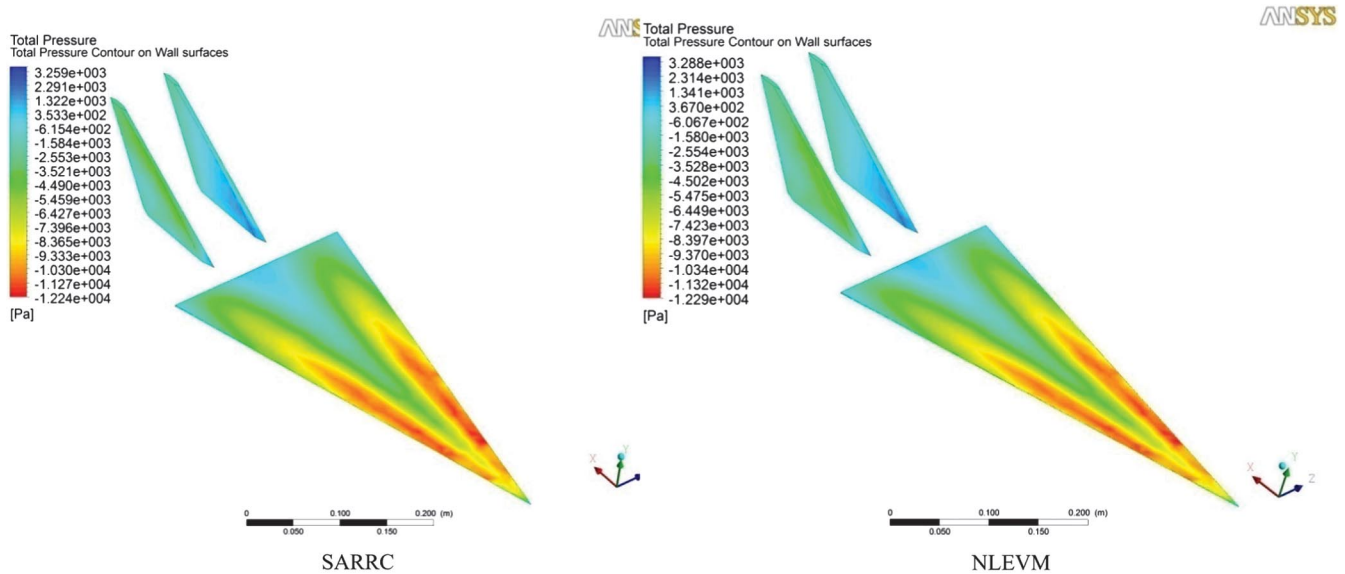

SARRC NLEVM

Fig. 3 Total pressure contours on wing upper surface and tails.

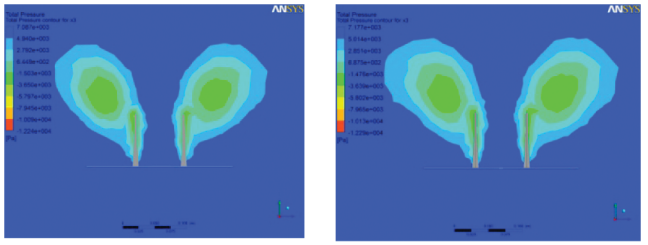

SARRC NLEVM

Fig. 6 Total pressure contours at $x = 0.62$ m.

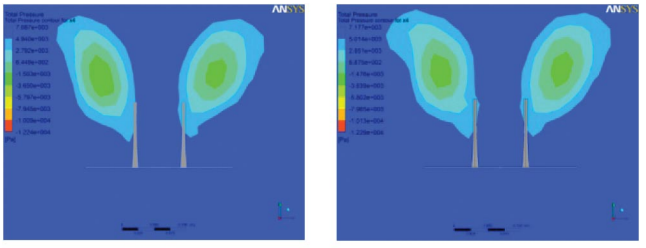

SARRC NLEVM

Fig. 7 Total pressure contours at $x = 0.7$ m.

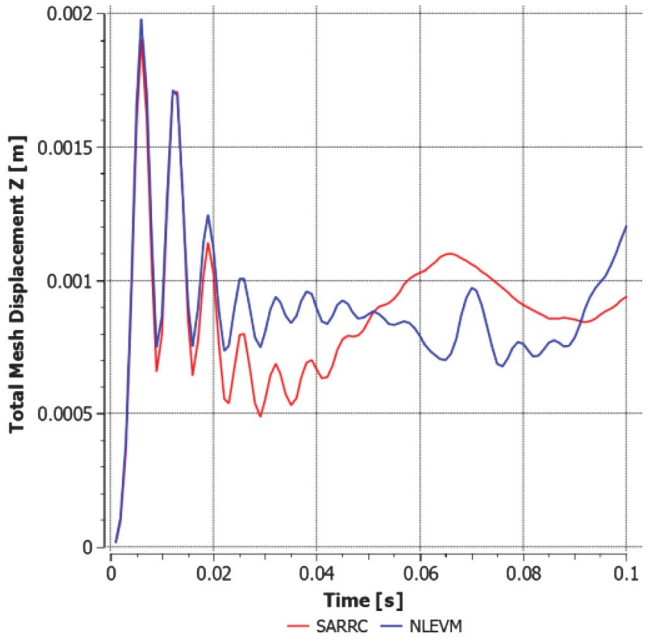

Fig. 8 Time history of the rear tip Z direction displacement.

B. Results for Unsteady RANS, Two-Way Fluid–Structure Interaction Case

The two-way fluid–structure interaction simulations have been conducted for 0.1 s using SARRC and NLEVM turbulence models with 0.001 s time step. This time step selection was done by optimizing the available computational power to the author. It should be noted that the present investigation is the first ever study of tail buffet problem with a two-way fluid–structure interaction and using the two advanced nonlinear eddy viscosity turbulence models: NLEVM and SARRC.

The time history of the rear tip displacement for the two turbulence models of the right tail is shown in Fig. 8.

The amplitude and frequency of vibration are similar for both turbulence models at the beginning until 0.02 s and both of them are close to being periodic. Afterward they start to deviate and both show a lack of periodicity. The unsteady nature of the vibration of the tail tip can be noticed.

The time histories of the surface pressure are used to calculate the differential pressure as the difference between the inner and the outer surface total pressure values on the right tail. These values are RMS averaged. Shown in Table 2 are the comparisons with the experimental data [23] of the computed RMS nondimensional pressure difference at the five specified transducer locations of the inner and outer surfaces of the right tail. A good agreement between the SARRC and NLEVM turbulence models is observed considering the relatively short physical computational time. Both SARRC and NLEVM turbulence model computations differ from the experimental data with an average of 52.68 and 49.43%, respectively. The SA and standard k-ω turbulence model computations differ from the experimental data with an average of 108.58 and 91.18%, respectively. Overall, the NLEVM turbulence model gives a better agreement than other turbulence models. The error percentages for NLEVM (49.43%) and SARRC (52.68%) are still too high and the simulations should continue to compute at least five repeated cycles to reduce the error percentage and this will be done in future publications by the authors.

NLEVM model gives better pressure results, for two-way fluid–structure simulations, because of the smaller production of the turbulence in the vortex core. This leads to less vorticity diffusion, resulting in a stronger vortex. A stronger vortex indicates high velocity and low pressure within the vortex core.

A comparison of wall clock time per iteration and time to convergence for the four RANS turbulence models was conducted. The simulations for the comparisons were conducted for a steady one-way fluid–structure interaction simulation of the wing only. From Table 3, it is observed that the NLEVM turbulence model simulation is approximately 1.127, 1.167, and 1.18 times more computationally expensive to iterate than the k-ω, SARRC, and SA turbulence models, respectively. Also observed in Table 3 is that NLEVM turbulence model simulation is approximately 1.113, 1.154, and 1.1176 times more computationally expensive to converge than the k-ω, SARRC, and SA turbulence models, respectively. Both k-ω and NLEVM are two-equation turbulence models and more

Table 2 Comparison of the computed RMS nondimensional pressure difference at the five specified transducer locations of the inner and outer surfaces of the right tail for the unsteady RANS, two-way fluid–structure interaction cases for a total simulation time of 0.1 s

	1	2	3	4	5	Difference average
EXP	0.0900	0.0630	0.1708	0.1673	0.0340	
SA + vorticity	0.013733	0.052966	0.189492	0.258752	0.000971	
% Difference	84.74104	15.92638	10.94361	54.66351	97.14304	52.68
NLEVM	0.011611	0.070445	0.164325	0.244311	0.00069	
% Difference	87.09938	11.81701	3.790949	46.03162	97.97148	49.34
SA	0.001712	0.000252	0.269933	0.485218	0.000971	
% Difference	98.09734	99.59942	58.04029	190.0289	97.14304	108.58
k-ω	0.003491	0.034186	0.084374	0.128641	0.11571	
% Difference	96.12065	45.7372	50.60069	23.10755	240.323	91.18

Table 3 One-way fluid–structure interaction wing only case

	SA	SARRC	k-ω	NLEVM
Physical time for 1 iteration, s	57.18	58.26	60.3	68
Wall clock time for 1 iteration, s	36.34	37.29	39.55	44.14
Physical total time to convergence, hr	4.76	4.85	5.03	5.60

Comparison of the simulation wall clock time per iteration and physical time to converge for the four turbulence models.

computationally expensive than the one-equation turbulence models, SA and SARRC. SARRC turbulence model is based on the one-equation turbulence model, the SA model. Moreover, the SA model coefficient was derived from experimental data for types of flow that is different from the vortical flow of this problem. A one-equation turbulence model provides one independent transport equation for the undamped eddy viscosity. The NLEVM turbulence model is based on the two-equation turbulence model, Wilcox k-ω. The two-equation turbulence model provides two independent transport equations for the dissipation and the turbulent kinetic energy. With the specification of these two variables, two-equation models can capture more flow characteristics when compared with the one-equation turbulence models. NLEVM turbulence model involves the solutions of two transport equation compared with one equation for SARRC turbulence model as shown in Table 3.

V. Conclusions

A computational model for the prediction of the unsteady aeroelastic behavior of a flexible tail under buffet-induced loads has been developed. The unsteady Reynolds-averaged Navier–Stokes equations with four turbulence models have been used to model the flow and finite element analysis by using shell element to model the structural dynamics of the tail. The turbulence models are the standard linear Wilcox k-ω, nonlinear eddy viscosity model (NLEVM), Spalart–Allmaras, and SARRC. The modified Spalart–Allmaras model (SARRC) with a rotation/curvature-based production and curvature treatment is based on the corrections proposed by Mariani et al. [16,17], Spalart and Shur [14], and Shur et al. [15]. NLEVM is based on the standard Wilcox k-ω model and use the formulation of an explicit algebraic Reynolds stress model proposed by Wallin and Johansson [8] and Hellsten [9] to model the Reynolds stresses. The experimental data used for comparison are from Washburn et al. [23]. Washburn et al. obtained data on a simplified geometry: Mach 0.3 flow past a 76 deg delta wing pitched to 30 deg angle of attack. Two vertical tails were placed downstream of the delta wing [27,28].

The present work is the first ever study of tail buffet problem with a two-way fluid–structure interaction and using the two nonlinear eddy viscosity turbulence models: NLEVM and SARRC. The steady-state, time-averaged, one-way fluid–structure interaction case indicates that the results of the four turbulence models, SA, standard linear Wilcox k-ω, NLEVM, and SARRC, do not compare well with the experimental data. These results are somewhat expected for the steady-state, one-way simulation, because it involves no force and displacement transfer between the fluid and structure solvers.

For the unsteady two-way fluid–structure interaction case, the four models result in much favorable agreement with the experimental data. Results from the NLEVM model produce improved total pressure values on the tail as compared with the results from the other models.

Therefore, it is concluded that the buffet problem should be modeled and simulated as a two-way fluid–structure interaction. Also, NLEVM turbulence model is recommended, if compared with the other considered method, in predicting vortical flow characteristics over a delta wing. This is particularly necessary to predict the pressure values not only over the aircraft's surfaces but also on the tails because they experience the wake of the vortices.

References

[1] Levinski, O., "Vertical Tail Dynamic Response in Vortex Breakdown Flow," Air Vehicles Div., Platforms Sciences Lab., Dept. of Defense, Australian Government, Research Rept. DSTO-RR-0256, June 2003.

[2] Canfield, R. A., Morgenstern, S. D., and Kunz, D. L., "Alleviation of Buffet-Induced Vibration Using Piezoelectric Actuators," *Computers and Structures*, Vol. 52, Nos. 6, 2008, pp. 281–291. doi:10.1016/j.compstruc.2007.02.027

[3] Hanagud, S., Bayon de Noyer, M., Luo, H., Henderson, D., and Nagaraja, K. S., "Tail Buffet Alleviation of High-Performance Twin-Tail Aircraft Using Piezostack Actuators," *AIAA Journal*, Vol. 40, No. 4, 2002, pp. 619–627. doi:10.2514/2.1718

[4] Moses, R. W., "Active Vertical Tail Buffeting Alleviation on a Twin Tail Fighter Configuration in a Wind Tunnel," *CEAS International Forum on Aeroelasticity and Structural Dynamics*, NASA Langely Reseacrch Center, Hampton, VA, 1997.

[5] Cummings, R. M., Forsythe, J. R., Morton, S. A., and Squires, K. D., "Computational Challenges in High Angle of Attack Flow Prediction," *Progress in Aerospace Sciences*, Vol. 39, No. 5, July 2003, pp. 369–384. doi:10.1016/S0376-0421(03)00041-1

[6] Brandsma, F. J., Kok, J. C., Dol, H. S., and Elsenaar, A., "Leading Edge Vortex Flow Computations and Comparison with DNW-HST Wind Tunnel Data," *RTO/AVT Vortex Flow Symposium*, National Aerospace Lab., Amsterdam, May 2001.

[7] Gordnier, R. E., "Computational Study of a Turbulent Delta Wing Flowfield Using Two-Equation Turbulence Models," AIAA Paper 1996–2076, 1996.

[8] Wallin, S., and Johansson, A., "An Explicit Algebraic Reynolds Stress Model for Incompressible and Compressible Turbulent Flows," *Journal of Fluid Mechanics*, Vol. 403, Jan. 2000, pp. 89–132. doi:10.1017/S0022112099007004

[9] Hellsten, A., "New Advanced k–w Turbulence Model for High-Lift Aerodynamics," *AIAA Journal*, Vol. 43, No. 9, 2005, pp. 1857–1869. doi:10.2514/1.13754

[10] Dol, H. S., Kok, J. C., and Oskam, B., "Turbulence Modelling for Leading Edge Vortex Flows," AIAA Paper 2002-0843, 2002.

[11] Schiavetta, L. A., and Badcock, K. J., "Comparison of DES and URANS for Unsteady Vortical Flows Over Delta Wings," AIAA Paper 2007-1085, 2007.

[12] Dacles-Mariani, J., Zilliac, G. G., Chow, J. S., and Bradshaw, P., "Numerical/Experimental Study of a Wingtip Vortex in the Near Field," *AIAA Journal*, Vol. 33, No. 9, 1995, pp. 1561–1568. doi:10.2514/3.12826

[13] Dacles-Mariani, J., Kwak, D., and Zilliac, G. G., "On Numerical Errors and Turbulence Modeling in Tip Vortex Flow Prediction," *International Journal for Numerical Methods in Fluids*, Vol. 30, No. 1, 1999, pp. 65–82. doi:10.1002/(ISSN)1097-0363

[14] Spalart, P. R., and Shur, M. L., "On the Sensitization of Turbulence Models to Rotation and Curvature," *Aerospace Science and Technology*, Vol. 1, No. 5, 1997, pp. 297–302. doi:10.1016/S1270-9638(97)90051-1

[15] Shur, M. L., Strelets, M. K., Travin, A. K., and Spalart, P. R., "Turbulence Modeling in Rotating and Curved Channels: Assessing the Spalart-Shur Correction," *AIAA Journal*, Vol. 38, No. 5, 2000, pp. 784–792. doi:10.2514/2.1058

[16] Morton, S. A., Forsythe, J., Mitchell, A. M., and Hajek, D., "DES and RANS Simulations of Delta Wing Vortical Flows," AIAA Paper 2002-0587, 2002.

[17] Mellor, G. L., and Herring, H. J., "A Survey of the Mean Turbulent Field Closure Models," *AIAA Journal*, Vol. 11, No. 5, 1973, pp. 590–599. doi:10.2514/3.6803

[18] Rumsey, C. L., Gatski, T. B., and Morrison, J. H., "Turbulence Model Predictions of Extra-Strain Rate Effects in Strongly-Curved Flows," AIAA Paper 1999-0157, 1999.

[19] Menter, F. R., "Improved Two-Equation k-w Turbulence Models for Aerodynamic Flows," NASA TM-103975, Oct. 1992.

[20] *ANSYS Fluent Theory Guide*, ANSYS, Inc., Canonsburg, PA, Nov. 2011.

[21] Morton, S. A., Forsythe, J., Mitchell, A. M., and Hajek, D., "Detached Eddy Simulation and Reynolds Averaged Navier-Stokes Simulations of Delta Wing Vortical Flow Fields," *Journal of Fluids Engineering*, Vol. 124, No. 4, Dec. 2002, pp. 924–932. doi:10.1115/1.1517570

[22] *System Coupling User's Guide*, ANSYS, Inc., Canonsburg, PA, Nov. 2011.

[23] Washburn, A. E., Jenkins, L. N., and Ferman, M. A., "Experimental Investigation of Vortex-Fin Interaction," AIAA Paper 1993-0050, 1993.

[24] Sheta, E. F., "Computational Investigation and Validation of Twin-Tail Buffet Response Including Dynamics and Control," Ph.D. Dissertation, Aerospace Engineering Dept., Old Dominion Univ., Norfolk, VA, 1998.
[25] Meyn, L. A., James, K. D., and Geenen, R. J., "Correlation of F/A-18 Tail Buffet Results," *High-Alpha Projects & Technology Conference*, NASA Dryden Flight Research Center, Palmdale, CA, July 1994.
[26] Moses, R. W., and Pendleton, E., "A Comparison of Pressure Measurements Between a Full-Scale and a 1/6-Scale F/A-18 Twin Tail During Buffet," NASA TM-110282, 1996.
[27] Elmekawy, A., "Fluid-Structure Interaction Modeling of a F/A-18 Twin-Tail Buffet Using Non-Linear Eddy Viscosity Models," Ph.D. Dissertation, Aerospace Engineering Dept., Old Dominion Univ., Norfolk, VA, 2014.
[28] Elmekawy, A., Kandil, O. A., and Baysal, O., "F/A-18 Twin-Tail Buffet Modeling Using Non-Linear Eddy Viscosity Models," AIAA Paper 2014-2447, 2014.